Check for updates

Temperature dependence of the spin state and geometry in tricobalt paddlewheel complexes with halide axial ligands†

Anandi Srinivasan,[a,b] Xiaoping Wang, [ID] [c] Rodolphe Clérac, [ID] [a,b] Mathieu Rouzières,[a,b] Larry R. Falvello, [ID] [d] John E. McGrady [ID] [e] and Elizabeth A. Hillard [ID] *[a,b]

Trinuclear cobalt paddlewheel complexes, [Co$_3$(dpa)$_4$X$_2$] (dpa = the anion of 2,2′-dipyridylamine, X = Cl$^-$, Br$^-$, −NCS$^-$, −CN$^-$, (NC)$_2$N$^-$), are known to demonstrate a thermally-induced spin-crossover (SCO). Despite a wealth of structural and magnetic information about such complexes, the role of the axial ligand on the characteristic SCO temperature ($T_{1/2}$) remains ambiguous. The situation is complicated by the observation that the solid state geometry of the complexes, symmetric or unsymmetric, with respect to the central cobalt ion, also appears to influence the SCO behavior. In order to seek trends in the relationship between the nature of the axial ligand, geometry and magnetic properties, we have prepared the first examples of tricobalt paddlewheel complexes with axial fluorido and iodido ligands, as well as two new chlorido and bromido solvates. Their SCO properties are discussed in the context of an examination of previously reported chlorido and bromido adducts. The main conclusions are: (1) $T_{1/2}$ values follow the trend I$^-$ < Br$^-$ ≈ Cl$^-$ < F$^-$; (2) while the molecular geometry is predominantly guided by crystal packing for the Cl$^-$, Br$^-$ and I$^-$ derivatives, the presence of an axial fluoride may favor a more symmetric core; (3) the magnetic characterization of a second example of an unsymmetric complex supports the observation that they display dramatically lower $T_{1/2}$ values than their symmetric analogues; and (4) SCO in crystallographically symmetric compounds apparently occurs without loss of molecular or crystallographic symmetry, while a gradual geometric transformation linking the temperature dependence of quasi-symmetric to unsymmetric in crystallographically unconstrained compounds was found.

Introduction

Complexes consisting of three or more linearly-disposed metal ions, "extended metal atom chains" (EMACs) or "metal strings", have been intensively studied with respect to their electronic, magnetic, and single-molecule conductive

properties.[1–3] The simplest examples are trinuclear complexes supported by four 2,2′-dipyridylamine anions (dpa), where the axial positions are most often occupied by halide or pseudohalide ligands. Chromium and cobalt derivatives have the particularity of presenting either symmetric metal cores, where Δ_{M-M}, the difference between the intermetallic distances, is less than 0.05 Å,[1] or dramatically unsymmetric cores, where Δ_{M-M} has been found to reach up to 0.65 Å.[4] In trinuclear chromium complexes, the preferred geometry appears to depend on the nature of the axial ligands; stronger σ-donors tend to stabilize the symmetric arrangement and weaker donors the unsymmetric form.[5,6]

The effect of the axial ligand on the conformation of the tricobalt core is less well understood. Remarkably, [Co$_3$(dpa)$_4$Cl$_2$] can present a symmetric (*s*-[Co$_3$(dpa)$_4$Cl$_2$]) or unsymmetric core (*u*-[Co$_3$(dpa)$_4$Cl$_2$]), depending on the crystalline environment (Chart 1).[7,8] All evidence to date points to this variability being a solid state phenomenon; in solution, only *s*-[Co$_3$(dpa)$_4$Cl$_2$] has been detected,[9] while a Hirshfeld surface analysis demonstrated the importance of intermolecular interactions on the

[a]CNRS, CRPP, UMR 5031, 33600 Pessac, France.
E-mail: hillard@crpp-bordeaux.cnrs.fr
[b]Univ. of Bordeaux, CRPP, UMR 5031, F-33600 Pessac, France
[c]Neutron Scattering Division, Neutron Sciences Directorate,
Oak Ridge National Laboratory, Oak Ridge, TN, USA
[d]Dept. of Inorganic Chemistry and ICMA, Univ. of Zaragoza, Zaragoza, Spain
[e]Department of Chemistry, University of Oxford, Oxford, UK

†Electronic supplementary information (ESI) available: Thermal ellipsoid plot of **1**[BF$_4$]·4CH$_2$Cl$_2$, diagrams showing intramolecular interactions for **1**·2CH$_2$Cl$_2$, **3**·Et$_2$O and **4**·Et$_2$O, crystal data and refinement and selected bond distance and angles tables for newly reported compounds, χT *vs. T* plots and fits for previously reported compounds. CCDC 1865577–1865593 and 1877180–1877181. For ESI and crystallographic data in CIF or other electronic format see DOI: 10.1039/c8dt03833c
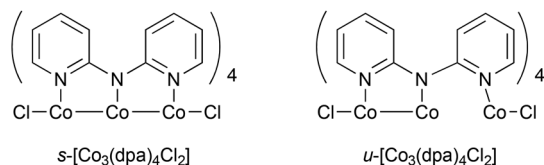
Chart 1

geometry of $[Co_3(dpa)_4Cl_2]$.[10] Geometric plasticity is not restricted to the chlorido adducts; in the case of $[Co_3(dpa)_4Br_2]$, for which three solvates have been crystallographically characterized, two of the structures are rigorously symmetric at room temperature, while the third is markedly unsymmetric.[11] Conversely, all of the reported complexes with stronger-field axial ligands ($-CN^-$, $-NCS^-$, $N(CN)_2^-$) are highly symmetric[12] suggesting that, like for the trichromium analogues, the ligand field may play a role in the core geometry.

This question is not purely academic, as it directly influences the spin-crossover (SCO) behaviour found in many tricobalt complexes.[7,8] For example, while the dichloromethane solvates of both s- and u-$[Co_3(dpa)_4Cl_2]$ show a thermally-induced SCO, there are significant differences in their solid state magnetic signatures. Symmetric $[Co_3(dpa)_4Cl_2] \cdot CH_2Cl_2$ was reported to display an $S = 1/2$ ground state with $g \approx 2.3$, and the temperature where 50% of the complexes are in the high spin state, $T_{1/2}$, equal to 329 K.[7] On the other hand, the unsymmetric form, $[Co_3(dpa)_4Cl_2] \cdot 2CH_2Cl_2$, presented a low-temperature plateau with $\chi T \approx 1$ cm^3 K mol^{-1}, indicating an $S = 1/2$ ground state with $g \approx 3.2$. This material displays a SCO at relatively low temperature, with an asymptotic curve reaching ~2.5 cm^3 K mol^{-1}, indicating significant population of the $S = 3/2$ excited state at high temperatures.[7]

If we ever hope to exploit the SCO properties of dpa-based tricobalt complexes, it is necessary to better understand the role of the ligand environment on the core geometry and magnetic behaviour. To this end, we have completed the series of halide adducts with the first examples of the fluorido and iodido complexes of $[Co_3(dpa)_4X_2]$, namely $[Co_3(dpa)_4F_2] \cdot 2CH_2Cl_2$, ($1 \cdot 2CH_2Cl_2$), $[Co_3(dpa)_4I_2] \cdot C_2H_4Cl_2$ ($4 \cdot C_2H_4Cl_2$) and $[Co_3(dpa)_4I_2] \cdot Et_2O$ ($4 \cdot Et_2O$). During this work, we also obtained new solvates of the chlorido and bromido adducts, $[Co_3(dpa)_4Cl_2] \cdot Et_2O$ ($2 \cdot Et_2O$) and $[Co_3(dpa)_4Br_2] \cdot Et_2O$ ($3 \cdot Et_2O$). To contextualize their structural and magnetic temperature dependence, we have examined the magnetic data for a number of previously reported chlorido[8] and bromido[11] adducts, and report the previously-undetermined thermodynamic parameters characterizing their SCO behaviour.

Experimental section

Materials

All reactions were carried out under an inert atmosphere of argon or nitrogen using standard Schlenk and glove box tech-

niques. Anhydrous $CoCl_2$ from Fisher Chemicals was stored at 120 °C, NaI and AgBF$_4$ from Alfa Aesar were dried under vacuum (10^{-3} mbar) for 12 h and stored in a glovebox, anhydrous tetrabutylammonium fluoride (TBAF) solution (1 M in THF) and CoBr$_2$ from Sigma Aldrich were stored in a nitrogen atmosphere. Dichloromethane (CH_2Cl_2), diethyl ether (Et_2O) and acetonitrile (MeCN) were purified using an Inert Technologies solvent purification system. Anhydrous dimethylformamide (DMF), n-hexane and 1,2-dichloroethane ($C_2H_4Cl_2$) were purchased from Acros and degassed prior to use. $[Co_3(dpa)_4Cl_2] \cdot nCH_2Cl_2$ ($n = 1$, 2) was prepared according to the literature procedure.[13]

Physical measurements

CHN elemental analyses were performed by the Service d'Analyse Elémentaire, UMR 7565, Université de Lorraine, France and by PLACAMAT, UMS 3626, Université de Bordeaux. IR spectra were measured on a Nicolet 6700 FT-IR using a Smart iTR accessory between 550 and 4000 cm^{-1}.

Crystallography

Single crystals suitable for X-ray diffraction were selected under immersion oil in ambient conditions and attached to a MiTeGen microloop. For structures at 350 K, the crystals were fixed to a pin using Apiezon AP101 grease. The crystals were mounted and centred in the X-ray beam using a video camera. Data collection was performed on a Bruker APEXII Quasar diffractometer with Mo Kα ($\lambda = 0.71073$ Å) radiation. The data were collected using a routine to survey reciprocal space, and were indexed by the APEX2 program.[14] Data were reduced and integrated using SAINT$^+$ (ref. 14) and an absorption correction was applied using SADABS.[15] The structures were solved using direct methods and refined by least-squares refinement on F^2 followed by difference Fourier synthesis.[16] All hydrogen atoms were introduced at idealized positions and were allowed to ride on the neighbouring atoms with relative isotropic displacement coefficients. Crystal and refinement data are given in Tables S1–S5.† Cif files have been deposited with the Cambridge Structural Database CCDC 1865577–1865593, 1877180 and 1877181.

Magnetic measurements

Magnetic measurements were carried out with an MPMS-XL Quantum Design SQUID magnetometer, working between 1.8 and 400 K with applied dc fields ranging from −7 to 7 T. Measurements were performed on freshly filtered polycrystalline samples of $1 \cdot 2CH_2Cl_2$ (22.97 mg), $2 \cdot Et_2O$ (20.82 mg), $3 \cdot Et_2O$ (22.10 mg), $4 \cdot C_2H_4Cl_2$ (17.94 mg) and $4 \cdot Et_2O$ (17.43 mg) sealed in a polypropylene bag (3 × 0.5 × 0.02 cm). Prior to the experiments, the field-dependent magnetization was measured at 100 K in order to confirm the absence of any bulk ferromagnetic impurities. The magnetic data were corrected for the sample holder and the intrinsic diamagnetic contributions.

Synthesis

[Co₃(dpa)₄F₂]·2CH₂Cl₂, 1·2CH₂Cl₂. Addition of AgBF₄ (0.070 g, 0.36 mmol) to a CH₂Cl₂ solution (15 mL) of [Co₃(dpa)₄Cl₂] (0.15 g, 0.16 mmol) afforded a dark green-brown solution that was stirred at room temperature for 16 h. The resulting solution was filtered over Celite and a 1 M THF solution of TBAF (0.48 mL, 0.48 mmol) was added dropwise to the filtrate. After standing overnight, dark brown crystals were filtered off and washed with hexane. Yield: 0.10 g (59%). Elemental analysis Calcd for $C_{42}H_{36}N_{12}Co_3Cl_4F_2$ (%): C 47.35, H 3.41, N 15.78 Found C 47.69, H 3.70, N 15.99. FT-IR ($\bar{\nu}$, cm^{-1}): 1602s, 1590s, 1546m, 1466w, 1450w, 1419m, 1360s, 1308s, 1281m, 1150s, 1053w, 1023s, 882m, 756m, 737m, 649w.

[Co₃(dpa)₄Cl₂]·Et₂O, 2·Et₂O‡. [Co₃(dpa)₄Cl₂] (0.05 g) was dissolved in DMF (5 mL) and filtered over Celite. Crystals were obtained from the DMF solution layered with diethyl ether within 4 days. Yield: 45 mg, (90%) Elemental analysis Calcd for $C_{44}H_{42}N_{12}Co_3Cl_2O$ (%): C 52.71, H 4.22, N 16.76 Found: C 52.85, H 4.50, N 16.47. FT-IR ($\bar{\nu}$, cm^{-1}): 1603s, 1591s, 1546m, 1468s, 1457s, 1416s, 1363s, 1313s, 1279m, 1251w, 1152s, 1104m, 1041w, 1018s, 932w, 884s, 779w, 762s, 740s, 639w, 565w.

[Co₃(dpa)₄Br₂]·Et₂O, 3·Et₂O. This reaction is a modification of that previously published for [Co₃(dpa)₄Br₂],[11] except that the resulting solid from the reaction was extracted with DMF. Crystals were obtained from the DMF solution layered with diethyl ether. Yield: 0.68 g (62%) Elemental analysis Calcd for $C_{44}H_{42}N_{12}Co_3Br_2O$ (%): C 48.42, H 3.88, N 15.40 Found: C 48.74, H 4.08, N 15.61. FT-IR ($\bar{\nu}$, cm^{-1}): 1603s, 1591s, 1546m, 1467s, 1456s, 1416s, 1362s, 1313s, 1279m, 1250w, 1164w, 1152s, 1104s, 1042w, 1018s, 964w, 933w, 885s, 843w, 761s, 739s, 647w, 563w.

[Co₃(dpa)₄I₂]·C₂H₄Cl₂, 4·C₂H₄Cl₂. [Co₃(dpa)₄Cl₂] (0.20 g, 0.22 mmol) and NaI (1.65 g, 11.0 mmol) were dissolved in MeCN (15 mL) and stirred at room temperature for 16 h. A deep red-brown solution and a white precipitate (NaCl) were obtained. The solvent was removed under vacuum and the solid was extracted with 1,2-dichloroethane. After standing overnight at −15 °C, red-brown crystals were collected and washed several times with hexane. Yield: 0.15 g (56%) Elemental analysis Calcd for $C_{42}H_{36}N_{12}Co_3I_2Cl_2$ (%): C 41.68, H 3.00, N 13.89 Found C 41.62 H 3.05 N 13.92. FT-IR ($\bar{\nu}$, cm^{-1}): 1603s, 1593s, 1547s, 1454s, 1418s, 1370s, 1313s, 1236w, 1162w, 1146m, 947w, 925m, 886s, 769m, 751m, 729m, 670m, 573w, 557w.

[Co₃(dpa)₄I₂]·Et₂O, 4·Et₂O. The reaction was carried out under similar conditions as for 4·C₂H₄Cl₂, but the solid was extracted with CH₂Cl₂ and filtered over Celite. The CH₂Cl₂ was then removed under vacuum and the remaining solid was extracted with acetonitrile and layered with diethyl ether to yield brown crystals. Yield: 0.19 g (73%) Elemental analysis Calcd for $C_{44}H_{42}N_{12}Co_3I_2O$ (%): C 44.58, H 3.57, N 14.18

Found C 44.92 H 3.38 N 14.37. FT-IR ($\bar{\nu}$, cm^{-1}): 1604s, 1591s, 1548m, 1455s, 1420s, 1368s, 1312s, 1167m, 1148s, 1107m, 1045w, 1017m, 1004w, 925w, 885m, 756s, 734s, 636s, 580w.

Results

Synthesis

The fluorido adduct [Co₃(dpa)₄F₂]·2CH₂Cl₂, 1·2CH₂Cl₂, was synthesized from [Co₃(dpa)₄(BF₄)₂], prepared *in situ* by combining AgBF₄ and [Co₃(dpa)₄Cl₂][13] in CH₂Cl₂ and stirring for several hours. The dark green solution was then filtered to remove AgCl and treated with tetrabutylammonium fluoride in THF, giving a deep orange solution, from which an orange solid crystallized rapidly as 1·2CH₂Cl₂ in 59% yield. Attempts to synthesize 1 directly from [Co₃(dpa)₄Cl₂] using 2 eq. of AgF gave a mixture of [Co₃(dpa)₄F₂] and [Co₃(dpa)₄Cl₂] complexes, while 3 eq. yielded a mixture of products, including the oxidized 1[BF₄]·4CH₂Cl₂, which was crystallographically characterized (Fig. S1, Tables S6 and S12†). Attempts to cleanly synthesize this latter compound by oxidation of 1·2CH₂Cl₂ with NOBF₄ were unsuccessful.

Compounds 2·Et₂O and 3·Et₂O were obtained from recrystallization of [Co₃(dpa)₄Cl₂] and [Co₃(dpa)₄Br₂],[11] respectively, from DMF/Et₂O.

The iodido adduct [Co₃(dpa)₄I₂], 4, was obtained from treating [Co₃(dpa)₄Cl₂] with a large excess of NaI in MeCN. After stirring overnight, the solvent was removed under reduced pressure and the reddish-brown solid was extracted with C₂H₄Cl₂. When the solution was cooled to −15 °C, brown needles of 4·C₂H₄Cl₂ were obtained in 56% yield. For 4·Et₂O, the solid was first extracted with CH₂Cl₂ and filtered to remove excess NaI and NaCl. The CH₂Cl₂ was in turn evaporated under reduced pressure, the solid extracted with MeCN and layered with Et₂O, yielding a crop of 4·Et₂O as brown plates in 73% yield.

Crystal structures

Diffraction data for crystals of 1·2CH₂Cl₂, 2·Et₂O, 3·Et₂O, 4·Et₂O and 4·C₂H₄Cl₂ were collected at a minimum of three temperatures from 85 K. Diagrams of the structures at 85 K are represented in Fig. 1 and selected bond distances are given in Tables 1–3.

The fluorido adduct 1·2CH₂Cl₂ crystallizes in the space group $C2/c$ with the tricobalt complex on a general position. The Co–Co distances are similar at 85 K, with a difference (Δ_{Co-Co}) of only 0.0109(8) Å, and the Co–Co and Co–F distances remain essentially constant with increasing temperature (Table 1). In the crystal packing, the dichloromethane molecules interact with the axial fluorido ions through C–H⋯F hydrogen bonds, forming a one-dimensional motif (Fig. S2†). Notably, the ligand–solvent interactions are not identical on both sides of the complex, and the closer contact between the dichloromethane molecule and fluorido ion is associated with the slightly longer Co–Co distance. This compound has the unusual feature of having quite similar Co–N$_{pyr}$ and Co–N$_{amide}$

‡The compound 2·Et₂O was reported as a communication to the Cambridge Structural Database by M. Shatruk, RefCode GOJRII.
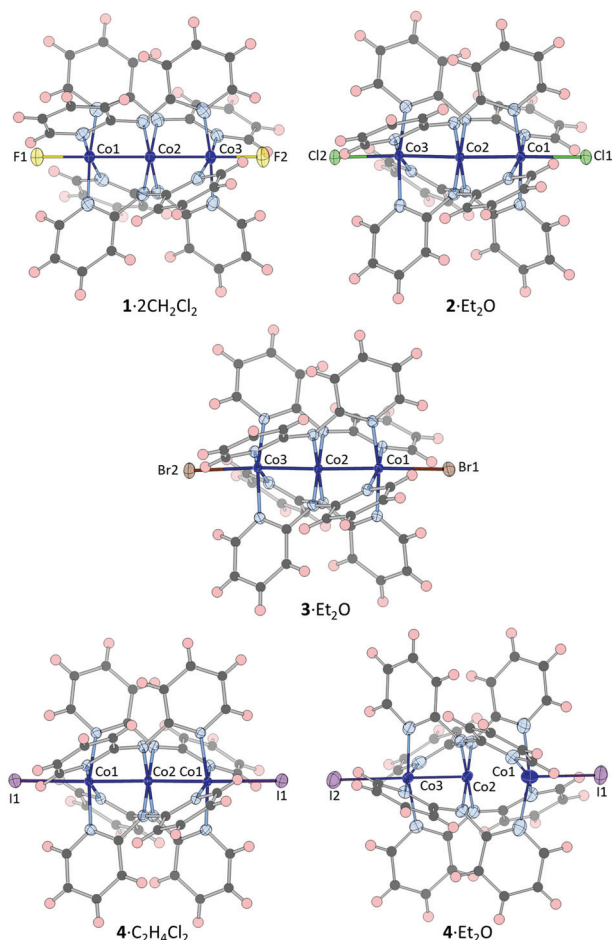
Fig. 1 Thermal ellipsoid (50%) representations of the new structures from X-ray diffraction data at 85 K. Solvents of crystallization have been omitted.

Table 1 Selected bond distances (Å) for **1**·2CH$_2$Cl$_2$

T (K)	85	120	250
Co(1)–Co(2)	2.3265(6)	2.3257(6)	2.3304(9)
Co(2)–Co(3)	2.3156(6)	2.3157(6)	2.3153(9)
Co(1)–F(1)	2.011(1)	2.0084(19)	2.016(3)
Co(3)–F(2)	2.005(1)	2.005(2)	2.007(3)

Table 2 Selected bond distances (Å) for **2**·Et$_2$O and **3**·Et$_2$O

T (K)	85	120	298	350
2·Et$_2$O				
Co(1)–Co(2)	2.3323(2)	2.3312(3)	2.3752(5)	2.3964(6)
Co(2)–Co(3)	2.3209(2)	2.3198(3)	2.3299(5)	2.3397(6)
Co(1)–Cl(1)	2.4816(4)	2.4823(4)	2.4574(7)	2.4350(9)
Co(3)–Cl(2)	2.4430(3)	2.4443(4)	2.4471(7)	2.4412(9)
3·Et$_2$O				
Co(1)–Co(2)	2.3303(2)	2.3295(2)	2.3691(6)	2.3862(7)
Co(2)–Co(3)	2.3162(2)	2.3162(2)	2.3218(5)	2.3308(7)
Co(1)–Br(1)	2.6852(2)	2.6890(2)	2.6363(6)	2.6096(7)
Co(3)–Br(2)	2.6167(2)	2.6205(2)	2.6081(6)	2.6002(7)

Table 3 Selected bond distances (Å) for **4**·Et$_2$O and **4**·C$_2$H$_4$Cl$_2$

4·Et$_2$O

T (K)	85	170	240	298
Co(1)–Co(2)	2.4295(3)	2.4504(8)	2.4645(4)	2.4680(15)
Co(2)–Co(3)	2.2942(3)	2.2928(8)	2.2937(4)	2.3047(14)
Co(1)–I(1)	2.7728(3)	2.7535(7)	2.7449(3)	2.7542(13)
Co(3)–I(2)	2.8620(3)	2.8620(7)	2.8719(3)	2.8702(13)

4·C$_2$H$_4$Cl$_2$

T (K)	85	120	298
Co(1)–Co(2)	2.3146(3)	2.3111(4)	2.3558(5)
Co(1)–I(1)	2.8904(4)	2.8925(4)	2.8447(6)

distances (Table S7†); all other known examples of tricobalt EMACs have much shorter Co–amide distances with respect to the Co–pyridine distances.

[Co$_3$(dpa)$_4$Cl$_2$]·Et$_2$O (**2**·Et$_2$O) and [Co$_3$(dpa)$_4$Br$_2$]·Et$_2$O (**3**·Et$_2$O) are isostructural, crystallizing in the space group $P2_1/c$, with almost equal Co–Co distances at 85 K ($\Delta_{\text{Co–Co}}$ = 0.0114(3) and 0.0141(3) Å, respectively, Table 2). The slight asymmetry of the trimetallic core is associated with pairwise X···H–C interactions between neighbouring molecules in the crystal packing (Fig. S3†). The two complexes display the same temperature dependence; specifically, both the longer Co–Co distance and the longer Co–N distances increase with increasing temperature, while the other Co–Co and Co–N distances remain essentially the same (Tables 2, S8 and S9). However, this divergence does not hold with respect to the Co–Cl and Co–Br distances, which are more alike at 350 K ($\Delta_{\text{Co–X}}$ = 0.006(1) and 0.009(1) Å) than at 85 K ($\Delta_{\text{Co–X}}$ = 0.0386(5) and 0.0685(3) Å).

Two [Co$_3$(dpa)$_4$I$_2$] solvates were crystallographically characterized. Compound **4**·Et$_2$O ($C2/c$) has highly dissimilar Co–Co distances at 85 K with $\Delta_{\text{Co–Co}}$ = 0.1353(4) Å (Table 3). This asymmetry is associated with a short contact of *ca.* 3 Å between the iodido ligand coordinated to the cobalt ion participating in the long Co–Co distance and the ether solvent (Fig. S4†), reminiscent of the asymmetric solvent interactions observed in [Co$_3$(dpa)$_4$Cl$_2$]·2CH$_2$Cl$_2$.[10] The temperature dependence of **4**·Et$_2$O is characterized by an increase of the asymmetry due to a divergence of the Co–Co, Co–I and average terminal Co–N bond distances with increasing temperature. This asymmetrization implicates only one half of the molecule: the longer Co–Co and terminal Co–N (Table S10†) distances increase and the shorter Co–I distance decreases from 85 to 298 K, while the other distances do not change substantially. In this way, the bond distances in **4**·Et$_2$O are highly dissimilar at 298 K, although they are still far from convergence at 85 K. It should be noted that this is the same trend previously observed in the unsymmetric chlorido adduct **2**·2CH$_2$Cl$_2$,[7] although it is less pronounced in the iodido adduct.

The central cobalt ion in **4**·C$_2$H$_4$Cl$_2$ is bisected by a 2-fold rotation axis, yielding crystallographically equivalent Co–Co, Co–X and terminal average Co–N distances. The complex in

$4 \cdot C_2H_4Cl_2$ exhibits a non-negligible increase of 0.0412(6) Å in the Co–Co distance from 85 to 300 K. This modification is concomitant with an increase in the average terminal Co–N distance (Table S11†) and a decrease in the Co–I distance with increasing temperature. This structural temperature dependence has been previously observed in the likewise rigorously symmetric compounds $2 \cdot$THF and $2 \cdot$cyclohexane, both of which show a thermally-induced SCO.[8] We will revisit the relationship between the structural temperature dependence and the SCO in the discussion section.

Temperature dependence of the magnetic susceptibility

Variable temperature dc magnetic susceptibility measurements were carried out on freshly-filtered polycrystalline samples of $1 \cdot 2CH_2Cl_2$, $2 \cdot Et_2O$, $3 \cdot Et_2O$, $4 \cdot Et_2O$ and $4 \cdot C_2H_4Cl_2$ from 1.85 K to a maximum temperature dictated by the respective thermal stability of the compounds, as determined by verifying the reversibility of the curves above 300 K (Fig. 2). As shown in the χT vs. T plots, all compounds exhibit a low temperature plateau around 0.55 cm³ mol⁻¹ K, corresponding to a doublet ground state with g values of ca. 2.4. The magnetic susceptibility data were fit to the ideal solution model (eqn (1)),[17] with $S_{LS} = 1/2$ and $S_{HS} = 3/2$. The resulting thermodynamic parameters are given in Table 4. To complement these results, the thermodynamic parameters from a (re)fitting of the magnetic data for several previously-reported compounds have been included (χT vs. T plots are presented in Fig. S5 and S6†). As the value of χT_{HS} could not always be determined from the experimental data and taking $4 \cdot C_2H_4Cl_2$ as a reference, the g_{HS} value was fixed at 2.66 for all compounds except $4 \cdot Et_2O$, $4 \cdot C_2H_4Cl_2$ and $2 \cdot 2CH_2Cl_2$. The ΔH, $T_{1/2}$ and g_{LS} parameters were allowed to refine freely.

$$\chi T = \frac{\chi T_{HS} - \chi T_{LS}}{1 + \exp\left(\frac{\Delta H}{R}\left(\frac{1}{T} - \frac{1}{T_{\frac{1}{2}}}\right)\right)} + \chi T_{LS}. \quad (1)$$
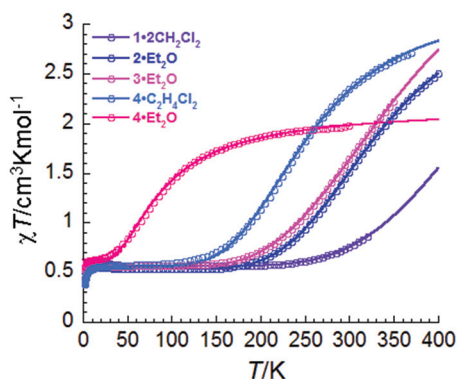
Fig. 2 χT versus T plots at 1000 Oe for the newly reported compounds, χ being the molar magnetic susceptibility defined as M/H. Lines are the fits to the ideal solution model (eqn (1)).

Discussion

In this study, we wished to explore the relationship between the axial ligand, the molecular geometry and the spin-crossover properties of dpa-based tricobalt EMACs. We will approach these questions in succession, and first examine the role of the axial ligand on the molecular geometry. Based on the data presented here and found in the literature, there does not appear to be a correlation between the nature of the axial ligand and the molecular geometry for the chlorido, bromido and iodido adducts, which, at room temperature, range from rigorously symmetric to quite unsymmetric, depending on the solvent of crystallization. Concerning the fluorido adduct, so far only one example is known. In $1 \cdot 2CH_2Cl_2$, the difference in Co–Co distances, Δ_{Co-Co}, is less than 0.05 Å, and this complex

Table 4 Thermodynamic parameters from fitting of the magnetic susceptibility data to the ideal solution model (eqn (1))

	ΔH (kJ mol⁻¹)	ΔS (J mol⁻¹ K⁻¹)	g_{LS}	g_{HS}	$T_{1/2}$ (K)
$1 \cdot 2CH_2Cl_2$	18.6(5)	40.4	2.45(5)	2.66[a]	460(10)
$2 \cdot Et_2O$	14.6(5)	43.6	2.39(5)	2.66[a]	335(5)
$3 \cdot Et_2O$	13.3(5)	40.9	2.44(5)	2.66[a]	325(5)
$4 \cdot Et_2O$	1.5(2)	12.3	2.59(5)	2.32(5)	122(5)
$4 \cdot C_2H_4Cl_2$	9.5(5)	36.5	2.45(5)	2.66(5)	260(5)
$2 \cdot CH_2Cl_2$	18.0[b]	54.7[b]	2.35(2)[b]	2.35(2)[b]	329[b]
	16.0(5)	44.8	2.39(5)	2.66[a]	357(5)
$2 \cdot 2CH_2Cl_2$	n.r.[b]	n.r.[b]	3.21(2)[b]	2.51(2)[b]	n.r.[b]
	1.6(2)	8.3	3.37(5)	2.76(5)	193(5)
$2 \cdot 1.75C_7H_8 \cdot 0.5C_6H_{14}$[c]	6.6(5)	28.7	2.41(5)	2.66[a]	230(5)
$2 \cdot C_4H_8O$[c]	11.6(5)	39.7	2.37(5)	2.66[a]	292(5)
$2 \cdot C_6H_6$[c]	12.6(5)	43.6	2.36(5)	2.66[a]	289(5)
$2 \cdot C_6H_{12}$[c]	9.1(5)	33.3	2.46(5)	2.66[a]	273(5)
$3 \cdot CH_2Cl_2$[d]	14.9(5)	34.5	2.38(5)	2.66[a]	431(5)
$3 \cdot 1.75C_7H_8 \cdot 0.5C_6H_{14}$[d]	8.0(5)	33.2	2.41(5)	2.66[a]	241(5)
$3 \cdot C_6H_{12}$[d]	8.2(5)	40.4	2.49(5)	2.66[a]	203(5)

[a] g_{HS} was fixed in the fitting process. [b] Values from ref. 7. [c] Data from ref. 8. [d] Data from ref 11. n.r. = not reported.

is therefore considered "symmetric", or more precisely "quasi-symmetric", as Δ_{Co-Co}, while small, is nonzero.

These results, taken together, are consistent with the observation that the geometry of complexes with weaker axial ligands is sensitive to crystal packing, while the presence of relatively strong field axial ligands favours symmetric or quasi-symmetric structures. Specifically, the symmetry in $[Co_3(dpa)_4(CN)_2]\cdot CH_2Cl_2$ is crystallographically enforced, while all the known $-NCS^-$ and $N(CN)_2^-$ adducts have similar Co–Co distances, with the largest variation being 0.014 Å.[9] An alternative hypothesis concerning the fluorido adduct is that the low polarizability of this anion does not lend itself to significant interactions with other moieties that can distort the {Co₃} core. Undoubtedly, further examples of tricobalt complexes with axial fluorido ligands should be sought in an effort to clarify this observation.

The deconvolution of packing and electronic effects on the core geometry is unfortunately complicated by the lack of an isostructural series for the four halide analogues to date. While the chlorido and bromido adducts are often isostructural,[8,11] the fluorido and the iodido adducts do not follow the same pattern. For example, $1\cdot 2CH_2Cl_2$ ($C2/c$) is not isostructural with $2\cdot 2CH_2Cl_2$ ($I\bar{4}$), and while $2\cdot Et_2O$ and $3\cdot Et_2O$ ($P2_1/c$) are isostructural, the iodido adduct $4\cdot Et_2O$ ($C2/c$) is not. We can conclude that obtaining an isostructural series is not a trivial task, and may indeed be impossible, due to the varying sizes of the axial ligands under consideration. Nonetheless, for the isostructural pairs $2/3\cdot Et_2O$ and $2/3\cdot 1.75toluene\cdot 0.5hexane$, the core symmetries and temperature dependences within each pair are comparable. Likewise, their spin crossover properties are similar, with almost identical $T_{1/2}$ values, ~330 K for the diethyl ether solvates and ~235 K for the toluene/hexane solvates (Table 4). This observation suggests that the SCO behaviour in the chlorido and bromido adducts is principally a result of molecular geometry and crystal packing, and that the similar ligand field of the Cl^- and Br^- anions does not allow us to differentiate any electronic effect for these axial ligands.

Indeed, the important influence of the molecular geometry on the spin-crossover properties has been previously observed in the disparate behaviour of the respective symmetric and unsymmetric complexes $2\cdot CH_2Cl_2$ and $2\cdot 2CH_2Cl_2$.[7] We now have a second comparative example in the form of two iodido complexes, where the dichloroethane solvate is rigorously symmetric and the diethyl ether solvate is unsymmetric. From Fig. 3, which collects the $T_{1/2}$ values for all measured compounds, it can be seen that the $T_{1/2}$ values for the unsymmetric $2\cdot 2CH_2Cl_2$ and $4\cdot Et_2O$ (in red) are significantly lower than those of their more symmetric analogues.

While there is considerable overlap between the series, the $T_{1/2}$ values generally follow the trend $F^- > Cl^- \approx Br^- > I^-$. The impact of the fluorido ligands in stabilizing the $S = 1/2$ spin state has been previously seen in a series of one-dimensional polymers of alternating $[(Co_3(dpa)_4)]^{2+}$ and MF_6^{2-} units, which also demonstrated very high spin-crossover temperatures ($T_{1/2} > 400$ K).[18,19] It should also be mentioned that the structure of
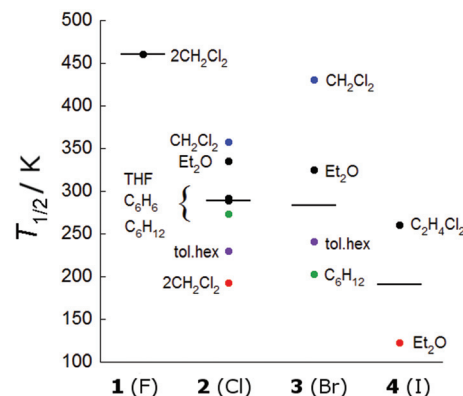

Fig. 3 Distribution of $T_{1/2}$ values for all reported compounds. Black lines represent the median and coloured dots are discussed in the text.

$1\cdot 2CH_2Cl_2$ does not display any significant geometric changes up to 250 K, a temperature where the compound remains fully in the low spin state, suggesting that our assumption that the changes in geometry are indeed representative of the spin-crossover phenomenon is reasonable.

A few compounds show anomalous behaviour and deserve further comment. The crystallographically symmetrical ($\Delta_{Co-Co} = 0$) $3\cdot CH_2Cl_2$ has an exceptionally high $T_{1/2}$ value compared to its congener $2\cdot CH_2Cl_2$ (431 K vs. 357 K, blue dots in Fig. 3). Although the two complexes are isostructural near room temperature, $2\cdot CH_2Cl_2$ undergoes a phase change which breaks the equivalence of the Co–Co distances at lower temperatures. But this does not explain the unusual temperature dependence observed in $3\cdot CH_2Cl_2$. Unlike the other rigorously symmetric compounds $2\cdot THF$, $2\cdot C_6H_{12}$, $3\cdot C_6H_{12}$ and $4\cdot C_2H_4Cl_2$ where the Co–X distance *decreases* with increasing temperature (Table 5), in $3\cdot CH_2Cl_2$, the Co–X distance significantly *increases* with temperature. The reason for this uncharacteristic temperature dependence is not clear from the packing diagrams, but is likely related to the unusual $T_{1/2}$ value, and theoretical calculations may help elucidate this behaviour.

Remaining within the crystallographically symmetric series, we note that $3\cdot C_6H_{12}$ displays a particularly low $T_{1/2}$ value compared to the chlorido analogue $2\cdot C_6H_{12}$ (203 K vs. 273 K, green dots in Fig. 3). These complexes are not isostructural and $2\cdot C_6H_{12}$ undergoes a phase transition between 120 and 213 K, which is clearly observable in the χT vs. T plot (Fig. S7†).

Table 5 Change in distances (in Å) with increasing T for compounds with crystallographically enforced symmetry at reported temperatures

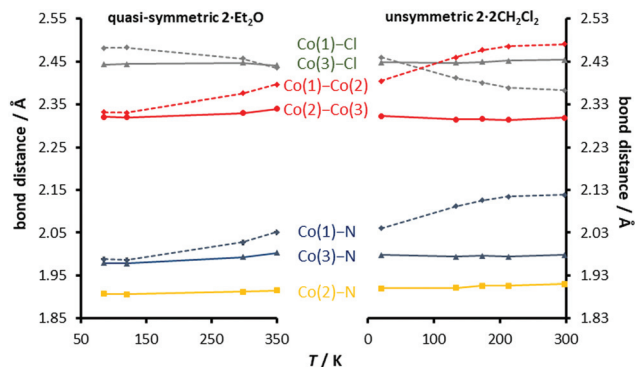|	$2\cdot THF$	$2\cdot C_6H_{12}$	$3\cdot C_6H_{12}$	$3\cdot CH_2Cl_2$	$4\cdot C_2H_4Cl_2$
δT (K)	120–295	213–295	110–298	111–240	85–298
Co(1)–Co(2)	0.037(1)	0.031(1)	0.064(1)	0.007(1)	0.041(1)
Co(1)–X(1)	−0.017(1)	−0.014(1)	−0.054(1)	0.043(1)	−0.046(1)
Co(1)–N$_{avg}$	0.038(3)	0.031(4)	0.060(3)	0.015(9)	0.042(3)
Co(2)–N$_{avg}$	0.009(3)	0.009(4)	0.011(3)	0.005(9)	0.006(3)
$T_{1/2}$ (K)	292(5)	273(5)	203(5)	431(5)	260(5)
Ref.		8		11	This work

Fig. 5 Comparison of the structural data from X-ray crystallography on two distinct crystals, the quasi-symmetric and unsymmetric forms of [$Co_3dpa_4Cl_2$].

To explore this idea, we plotted previously published structural data for unsymmetric $2\cdot2CH_2Cl_2$ and the new data from (quasi)-symmetric $2\cdot Et_2O$ in Fig. 5. The two data sets have been aligned (requiring an offset of 0.02 Å) to emphasize the point that the trends for $2\cdot Et_2O$ are simply an extrapolation of those for $2\cdot2CH_2Cl_2$. Interestingly, the crossing of the two independent Co–Cl distances, due to the gradual elongation of Co(1)–Cl(1) with decreasing temperature, is replicated in both compounds. The similarity of the temperature dependence not only suggests that the same states are implicated in the spin-crossover for both the (quasi)-symmetric and unsymmetric compounds, but provides experimental evidence for the shallow ^2B potential energy state proposed by Pantazis *et al.*,[21] which links the symmetric ^2A low spin state with the unsymmetric ^4B high spin state and accounts for the gradual geometric changes previously observed for $2\cdot2CH_2Cl_2$. In this view, the location of the complex on the ^2B surface at a given temperature determines both the $T_{1/2}$ value and the asymmetry of the core, a relationship which is consistent with experimental evidence for crystallographically unconstrained compounds. This can be contrasted with the temperature dependence of the crystallographically symmetrical complexes, which implies the existence of a low-lying *symmetrical* quartet state, which is not present in the current theoretical picture. Experimental and theoretical work on rigorously symmetrical complexes is underway.

Conclusions

The synthesis of fluorido and iodido adducts of tricobalt paddle-wheel complexes has been accomplished for the first time, allowing a more comprehensive investigation of the influence of the axial ligands on their core geometry and spin-crossover properties. Although the relationship between axial ligands, geometry and the spin-crossover properties is far from simple, several conclusions can be derived. While there is quite a bit of overlap in the $T_{1/2}$ values among the four halide series, the presence of iodido ligands tends to stabilize the high spin state compared to their congeners, while fluorido ligands favour a much higher $T_{1/2}$ value. The structural geometry of complexes with I^-, Br^- and Cl^- ligands appears to be mainly a function of the crystal packing, while the only example of a fluorido compound is quite symmetric. Higher asymmetry in the tricobalt core is associated with destabilization of the low spin state, as exemplified by lower $T_{1/2}$ values, suggesting a continuum of core geometries consistent with the previous theoretical calculations.

These conclusions are offered with the caveat that the picture could easily evolve with the discovery of new halide adducts, and work is currently focused on efforts to obtain genuinely unsymmetric examples in the fluorido and bromido series.

Conflicts of interest

There are no conflicts of interest to declare.

Acknowledgements

Notes and references

1 J. F. Berry in *Multiple Bonds between Metal Atoms*, ed. F. A. Cotton, C. A. Murillo and R. A. Walton, Springer, USA, 2005, pp. 669–706.

2 M. Majumdar and J. K. Bera, in *Macromolecules Containing Metal and Metal-Like Elements*, ed. A. Abd-El Aziz, C. E. Carraher, C. U. Pittman and M. Zeldin, John Wiley & Sons, Inc., 2009, vol. 9, pp. 182–253.

3 S.-A. Hua, M.-C. Cheng, C.-h. Chen and S.-M. Peng, *Eur. J. Inorg. Chem.*, 2015, **2015**, 2510.

4 F. A. Cotton, L. M. Daniels, C. A. Murillo and I. J. Pascual, *J. Am. Chem. Soc.*, 1997, **119**, 10223.

5 J. F. Berry, F. A. Cotton, T. Lu, C. A. Murillo, B. K. Roberts and X. Wang, *J. Am. Chem. Soc.*, 2004, **126**, 7082.

6 M. Spivak, V. Arcisauskaite, X. Lopez, J. E. McGrady and C. de Graaf, *Dalton Trans.*, 2017, **46**, 6202.

7 R. Clérac, F. A. Cotton, L. M. Daniels, K. R. Dunbar, K. Kirschbaum, C. A. Murillo, A. A. Pinkerton, A. J. Schultz and X. Wang, *J. Am. Chem. Soc.*, 2000, **122**, 6226.

8 R. Clérac, F. A. Cotton, L. M. Daniels, K. R. Dunbar, C. A. Murillo and X. Wang, *Inorg. Chem.*, 2001, **40**, 1256.

9 F. A. Cotton, C. A. Murillo and X. Wang, *Inorg. Chem.*, 1999, **38**, 6294.

10 R. D. Poulsen, J. Overgaard, A. Schulman, C. Østergaard, C. A. Murillo, M. A. Spackman and B. B. Iversen, *J. Am. Chem. Soc.*, 2009, **131**, 7580.

11 R. Clérac, F. A. Cotton, L. M. Daniels, K. R. Dunbar, C. A. Murillo and X. Wang, *J. Chem. Soc., Dalton Trans.*, 2001, 386.

12 R. Clérac, F. A. Cotton, S. P. Jeffery, C. A. Murillo and X. Wang, *Inorg. Chem.*, 2001, **40**, 1265.

13 F. A. Cotton, L. M. Daniels, G. T. Jordan IV and C. A. Murillo, *J. Am. Chem. Soc.*, 1997, **119**, 10377.

14 *Bruker APEX2, SAINT+*, Bruker AXS Inc., Madison, Wisconsin, USA, 2012.

15 *Bruker SADABS*, Bruker AXS Inc., Madison, Wisconsin, USA, 2001.

16 G. M. Sheldrick, *Acta Crystallogr., Sect. C: Struct. Chem.*, 2015, **71**, 3–8.

17 O. Kahn, in *Molecular Magnetism*, VCH Publishers, New York, 1993, p. 59.

18 V. Bulicanu, K. S. Pedersen, M. Rouzières, J. Bendix, P. Dechambenoit, R. Clérac and E. A. Hillard, *Chem. Commun.*, 2015, **51**, 17748.

19 M. Cortijo, V. Bulicanu, K. S. Pedersen, M. Rouzières, J. Bendix, R. Clérac and E. A. Hillard, *Eur. J. Inorg. Chem.*, 2018, 320.

20 A. Hauser, J. Jeftic, H. Romstedt, R. Hinek and H. Spiering, *Coord. Chem. Rev.*, 1999, **190/192**, 471.

21 D. A. Pantazis and J. E. McGrady, *J. Am. Chem. Soc.*, 2006, **128**, 4128.